nanomaterials

MDPI

Review

Recent Advances of Solution-Processed Heterojunction Oxide Thin-Film Transistors

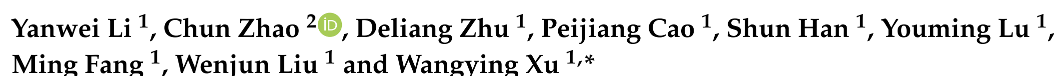

Yanwei Li [1], Chun Zhao [2], Deliang Zhu [1], Peijiang Cao [1], Shun Han [1], Youming Lu [1], Ming Fang [1], Wenjun Liu [1] and Wangying Xu [1,*]

[1] Shenzhen Key Laboratory of Special Functional Materials, College of Materials Science and Engineering, Guangdong Research Center for Interfacial Engineering of Functional Materials, Shenzhen University, Shenzhen 518060, China; yanweilo@163.com (Y.L.); dlzhu@szu.edu.cn (D.Z.); pjcao@szu.edu.cn (P.C.); hsdf52690@126.com (S.H.); ymlu@szu.edu.cn (Y.L.); m.fang@szu.edu.cn (M.F.); liuwj@szu.edu.cn (W.L.)

[2] Department of Electrical and Electronic Engineering, Xi'an Jiaotong-Liverpool University, Suzhou 215123, China; Chun.Zhao@xjtlu.edu.cn

* Correspondence: wyxu@szu.edu.cn

Received: 19 April 2020; Accepted: 13 May 2020; Published: 18 May 2020

Abstract: Thin-film transistors (TFTs) made of metal oxide semiconductors are now increasingly used in flat-panel displays. Metal oxides are mainly fabricated via vacuum-based technologies, but solution approaches are of great interest due to the advantages of low-cost and high-throughput manufacturing. Unfortunately, solution-processed oxide TFTs suffer from relatively poor electrical performance, hindering further development. Recent studies suggest that this issue could be solved by introducing a novel heterojunction strategy. This article reviews the recent advances in solution-processed heterojunction oxide TFTs, with a specific focus on the latest developments over the past five years. Two of the most prominent advantages of heterostructure oxide TFTs are discussed, namely electrical-property modulation and mobility enhancement by forming 2D electron gas. It is expected that this review will manifest the strong potential of solution-based heterojunction oxide TFTs towards high performance and large-scale electronics.

Keywords: heterojunction; metal oxide semiconductor; thin-film transistors; solution-processed

1. Introduction

Today, there is a growing demand for flat-panel displays with higher resolution, larger screen sizes, better viewing, and lower power consumption, pushing traditional amorphous silicon thin-film transistor (TFT) technology to its limits [1–3]. TFTs made of metal oxide semiconductors hold great promise in future display technology, owing to their high mobility, good transparency, and scalability [4–7]. Commercial metal oxides are grown via physical vapor deposition technologies, but solution-based approaches have been attracting particular attention recently [5,8–11]. Compared with conventional vacuum-based technologies, the solution approaches have additional advantages, including cost effectiveness, atmospheric fabrication, higher throughput, and material composition that is easy to tune [12–15]. Ways to reduce defect states and improve electrical performance and stability are an urgent challenge for solution-based metal oxide TFTs [16,17]. Various approaches have been taken to solve the above challenge, such as doping, modification of components, addition of additives, and novel post-treatments [9,18–20]. However, electron transport properties are still hindered by these defect-prone oxides [21–25].

A notable strategy has been recently developed to enhance the electrical performance of solution-derived oxide TFTs by utilizing heterojunction channels [26]. The schematic of the heterojunction oxide TFTs is demonstrated in Figure 1. It is revealed that heterostructures could

modulate electrical performance by taking advantage of both the front channel (providing high mobility) and the back channel (maintaining low off current) [27,28]. More importantly, some recent studies argue that the presence of a 2D electron gas system formed at the carefully engineered oxide heterointerface can greatly improve device mobility [24,29–33]. In this review, we summarize the recent progress of solution-processed heterostructure oxide TFTs. The heterojunction channel strategy could address the shortcomings of single-layer devices, providing a new route for future TFT technology development [34–36].

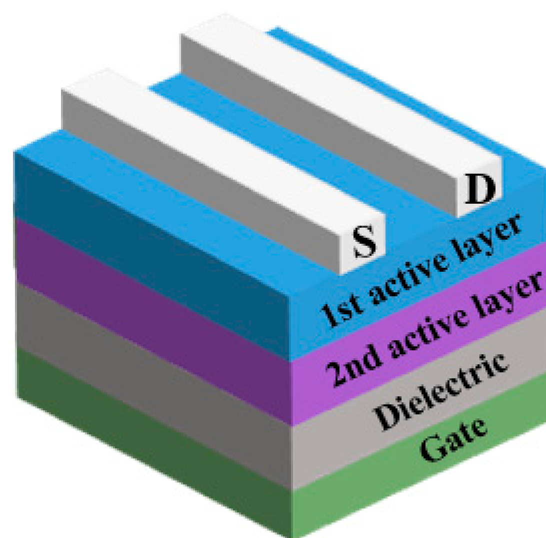

Figure 1. Cross-sectional view of the heterojunction oxide thin-film transistors (TFTs).

2. Heterojunction Oxide TFTs

2.1. Vacuum-Processed Heterojunction Oxide TFTs

Before reviewing solution-processed heterojunction oxide TFTs, we would like to make a short introduction on vacuum-based heterojunction oxide devices. In 2008, Kim et al. produced InSnO/GaInZnO (ITO/GIZO) heterojunction TFTs by magnetron sputtering, with a high mobility of 104 cm^2/Vs, a suitable threshold voltage (V_{th}) of 0.5 V, and a low V_{th} shift of 0.75 V for 4 h under 10 V bias voltage [37]. They found that the lower layer of highly conductive oxides could provide high mobility for the TFTs, while the upper layer of oxides with lower carrier concentration could adjust the threshold voltage. This new structure provides a new way to adjust the performance of TFTs. Subsequently, a number of scientists have studied and produced various excellent heterojunction oxide TFTs. In 2014, Chen et al. prepared InSnO/SnZnO (ITO/TZO) TFT on a glass substrate by taking advantage of ITO's higher carrier concentration and TZO's ability to control the charge conductance, and they obtained a high mobility of 105 cm^2/Vs [38]. In 2016, Cong et al. built quasi-double-channel (QDC) AlSnZnO (ATZO) TFTs with a superior mobility of 108 cm^2/Vs and an on/off ratio of 10^9 [36]. In 2019, He et al. prepared InGaZnO/In_2O_3 (IGZO/In_2O_3) TFTs by magnetron sputtering at room temperature, exhibiting high mobility (64.4 cm^2/Vs) and high on/off ratio (10^7), with large enhancement compared with single-layer IGZO and In_2O_3 TFTs [39]. They attributed this improvement to the defect self-compensation mechanism between the two layers. In 2019, Furuta et al. prepared IGZO/IGZO TFTs with a mobility of 24.7 cm^2/Vs and an on/off ratio of 10^7 [40]. Table 1 summarizes the recent progress in vacuum-processed heterojunction oxide TFTs. It can be observed that heterojunction oxide TFTs show excellent electrical properties, which are much better than those of the traditional single-layer device.

Table 1. Recent advances in vacuum-processed heterojunction oxide TFTs and representative single-layer devices.

Channel	Mobility ($cm^2 \cdot V^{-1} \cdot s^{-1}$)	*Ion/Ioff*	Subthreshold Swing	Dielectric	Year	Reference
ITO/GIZO	104	10^8	0.25	PECVD SiO_2	2008	[37]
ZTO/ITO	52	10^8	-	PECVD SiO_2	2010	[7]
IZO/IGZO	30	10^8	-	PECVD SiO_2	2010	[11]
H_xIZO/H_yIZO	15	10^{10}	-	Thermal SiO_2	2010	[3]
IGZO/GZO	10	10^7	0.93	Thermal SiO_2	2011	[6]
IGZO/ZIO	18	10^{10}	-	PECVD SiO_2	2011	[10]
ZTO/ITO	43	10^7	0.18	PECVD SiO_2	2011	[41]
HIZO/IZO	41.4	10^7	1.45	Thermal SiO_2	2011	[42]
IZO/GIZO	48	10^{10}	-	PECVD SiO_2	2012	[27]
HIZO/IZO	48	10^7	0.28	PECVD SiO_2	2012	[13]
IGZO/IGZO:Ti	63	10^6	0.73	HfO_2	2014	[22]
ZTO/IZO	32	10^8	0.20	PECVD SiO_2	2014	[23]
ITO/TZO	105	10^7	0.33	PECVD SiO_2	2014	[38]
In_2O_3/IZO	38	10^9	0.12	ZrO_2	2014	[24]
High-O-IGZO/Low-O-IGZO	60	10^8	0.2	Thermal SiO_2	2014	[34]
IZO/AZTO	53.2	10^{10}	0.15	PECVD SiO_2	2016	[12]
ZnO-H/ZnO	43	10^8	0.13	Thermal SiO_2	2016	[35]
L-AZTO/H-ATZO	108	10^9	0.15	PECVD SiO_2	2016	[36]
IG_XO/IG_YO	53.2	10^7	0.19	PECVD SiO_2	2017	[25]
AIZTO/IZO	53	10^{10}	0.15	PECVD SiO_2	2018	[32]
In_2O_3/IGZO	64.4	10^7	0.20	Thermal SiO_2	2019	[39]
In_2O_3/IGZO	67.5	10^7	0.08	HfO_2	2019	[39]
In_2O_3/IGZO	79.1	10^7	0.09	Si_3N_4	2019	[39]
ZnO(DEZ+O_3)/ZnO(DEZ+H_2O)	31.1	10^7	0.21	Al_2O_3	2019	[33]
IGZO/IGZO	24.7	10^7	0.1	Thermal SiO_2	2019	[40]
SnO_2	35.4	10^7	-	Thermal SiO_2	2015	[43]
ZnO	20	10^5	0.38	TiO_2/Al_2O_3	2015	[44]

2.2. *Solution-Processed Heterojunction Oxide TFTs*

Compared with conventional vapor-based techniques, solution processing (such as spin-coating, spraying, and printing) allows for the design and fabrication of novel oxide TFTs in a low-cost and straightforward fashion [43–45]. Many researchers have begun to study solution-grown heterojunction oxide TFTs. Table 2 and Figure 2 summarize the recent advances in solution-processed heterojunction oxide TFTs. For heterojunction oxide TFTs, we discuss two of the most prominent advantages, namely electrical-property modulation and mobility enhancement by forming 2D electron gas.

Table 2. Recent advances in solution-processed heterojunction oxide TFTs and representative single-layer devices.

Channel	Processing Temperature (°C)	Mobility ($cm^2 \cdot V^{-1} \cdot s^{-1}$)	I_{on}/I_{off}	Subthreshold Swing	Dielectric	Year	Reference
AIZO/IZO	350	1.57	10^7	0.59	SiO_2	2011	[26]
AIZO/IZO	350	5.62	10^6	0.53	SiO_2	2012	[46]
IGZO/IGZO	450	2.4	10^7	0.69	SiO_2	2013	[47]
ZTO/IGZO	450	2.09	10^7	0.49	SiO_2	2013	[48]
In_2O_3/IGO	250	2.6	10^8	-	SiO_2	2013	[49]
AIZO/IZO	350	23.4	10^7	0.27	SiO_2	2014	[50]
ITZO/IGZO	450	22.16	10^7	0.51	SiO_2	2014	[51]
ITZO/IGZO	450	40.03	10^5	0.12	ZrO_2	2014	[51]
QSL-III [1]	200	40	10^4	0.27	AlO_x/ZrO_x	2015	[52]
ZnO/SnO_2	300	15.4	10^7	-	SiO_2	2016	[53]

Table 2. *Cont.*

Channel	Processing Temperature (°C)	Mobility ($cm^2 \cdot V^{-1} \cdot s^{-1}$)	I_{on}/I_{off}	Subthreshold Swing	Dielectric	Year	Reference
In_2O_3/ZnO	400	48	10^4		SiO_2	2016	[54]
In_2O_3/ZnO	250	45	10^7	-	SiO_2	2017	[55]
In_2O_3/Li-ZnO	350	11.4	10^5	-	SiO_2	2017	[29]
ITZO/IGZO	350	38	10^8	0.41	SiO_2	2018	[30]
In_2O_3/PEI-In_2O_3 [2]	250	10	10^6	-	SiO_2	2018	[56]
In_2O_3/PEI-In_2O_3 [2]	250	30	10^6	-	ZrO_2	2018	[56]
In_2O_3/IGZO	400	14.5	10^6	-	SiO_2	2019	[17]
In_2O_3/ZnO-NPS/PS/ZnO	200	50.7	10^6	2.71	SiO_2	2019	[31]
IZIZ [3]	200	11.4	10^7	-	SiO_2	2019	[57]
Li-IZIZ [4]	200	25	10^8	-	AlO_x/ZrO_2	2019	[57]
AlInO/In_2O_3	300	40	10^7	0.7	SiO_2	2019	[58]
In_2O_3/In_2O_3	250	50	10^6	-	SiO_2	2019	[28]
IGZO	150	14	10^8	0.17	Al_2O_3	2012	[14]
InSmO	350	21.5	10^8	0.66	SiO_2	2020	[15]

[1] $In_2O_3/Ga_2O_3/ZnO/Ga_2O_3/In_2O_3$ (QSL-III). [2] Polyethylenimine-doped In_2O_3 (PEI-In_2O_3). [3] $In_2O_3/ZnO/In_2O_3/ZnO$ (IZIZ). [4] In_2O_3/ZnO-Li/In_2O_3/ZnO-Li (Li-IZIZ).

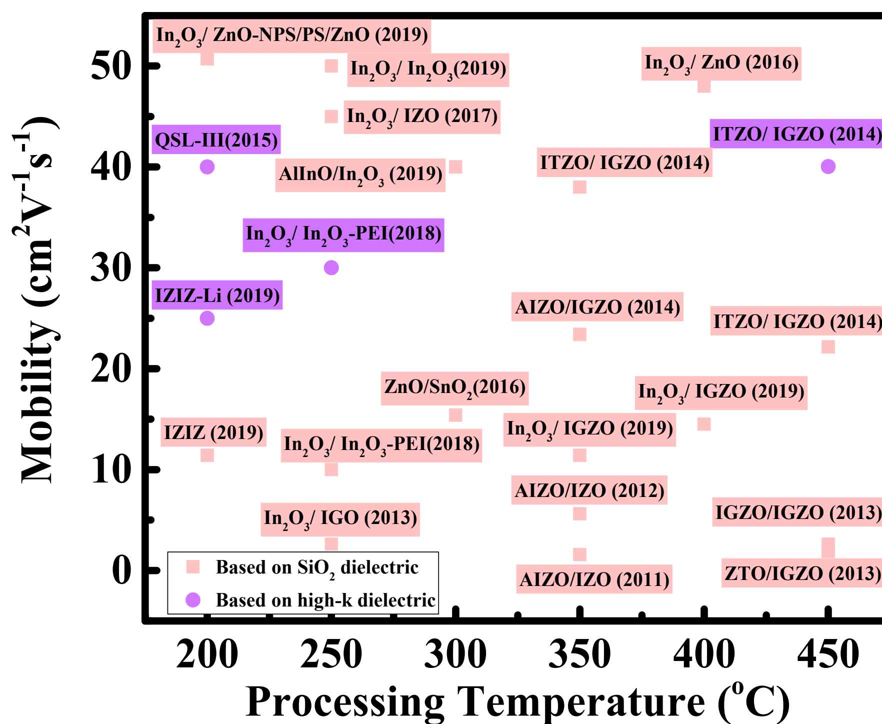

Figure 2. Mobility vs. processing temperature for solution-processed heterojunction oxide TFTs from Table 2 or high-k dielectrics. (QSL-III denotes $In_2O_3/Ga_2O_3/ZnO/Ga_2O_3/In_2O_3$; PEI-$In_2O_3$ denotes polyethylenimine-doped In_2O_3; IZIZ denotes $In_2O_3/ZnO/In_2O_3/ZnO$; Li-IZIZ denotes In_2O_3/ZnO-Li/In_2O_3/ZnO-Li.)

2.2.1. Electrical-Property Modulation

As a product of structural engineering technology, heterojunction oxide TFTs can take advantage of the excellent electrical properties of each layer [30,37]. As the front-channel layer has good conductivity, it can provide higher carrier concentration, thus forming maximum charge accumulation and finally achieving high mobility [10,41,42]. The carrier concentration in the back-channel layer is much lower than that of the front-channel layer, which leads to the difference in electron activation energy between the conduction band minimum and the Fermi energy level, forming an energy barrier at the interface [51]. Due to the existence of an energy barrier, the back-channel layer can effectively control the electron flow, thus reducing off current (I_{off}) and adjusting threshold voltage (V_{th}) [46]. A series

of representative papers show that heterojunction TFTs can achieve both high mobility and I_{off} by selecting suitable front- and back-channel materials.

In 2012, Jeong et al. adjusted the carrier concentration of the AlInZnO/InZnO (AIZO/IZO) interface and barrier height by changing the ratio of In/Zn in the IZO layer and the thickness of the IZO layer. The IZO layer could provide an enhanced mobility for the device due to its high electron concentration. Compared with the IZO layer, the AIZO layer had a larger E_C–E_F due to its lower carrier concentration, forming an energy barrier at the interface and reducing I_{off}. As the thickness of the conductive IZO layer decreased, the AIZO/IZO TFTs V_{th} shifted positive, and I_{off} decreased from 10^{-8} to 10^{-11} A. With a 12-nm-thick IZO layer, they obtained a device mobility of 5.63 cm^2/Vs and an on/off ratio of 10^6 [46]. For similar reports, refer to Kim et al. ZnSnO/InGaZnO (ZTO/IGZO), Yu et al. In_2O_3/InGaO (In_2O_3/IGO), Kim et al. InGaZnO/InGaZnO (IGZO/IGZO), Seo et al. AIZO/IZO, and Lee et al. In_2O_3/In_2O_3 (amorphous In_2O_3 and polycrystalline In_2O_3) [47–50].

Rim et al. boosted up the mobility of solution-processed oxide TFTs using an extremely thin layer of conductive InSnZnO (ITZO) inserted between the dielectric layer and the InGaZnO (IGZO) active layer [51]. The ITZO/IGZO TFTs have a high mobility (22.16 cm^2/Vs) and an excellent on/off current ratio (10^7). As shown in Figure 3a, the mobility of ITZO/IGZO is over ten times higher than that of single-layer IGZO (from 1.56 to 22.16 cm^2/Vs). At the front channel of ITZO, Sn^{4+} replaced In^{3+} to provide additional electrons to increase electron concentration, forming a highly conductive channel and providing high mobility for devices. Moreover, a barrier height (0.15 eV) between IGZO and ITZO (Figure 3b) could effectively modulate off current and threshold voltage. Nadarajah et al. (2015) also tried solution-processed ITZO/IGZO TFTs, showing a mobility of ~30 cm^2/Vs and an I_{on}/I_{off} of 10^6 [59].

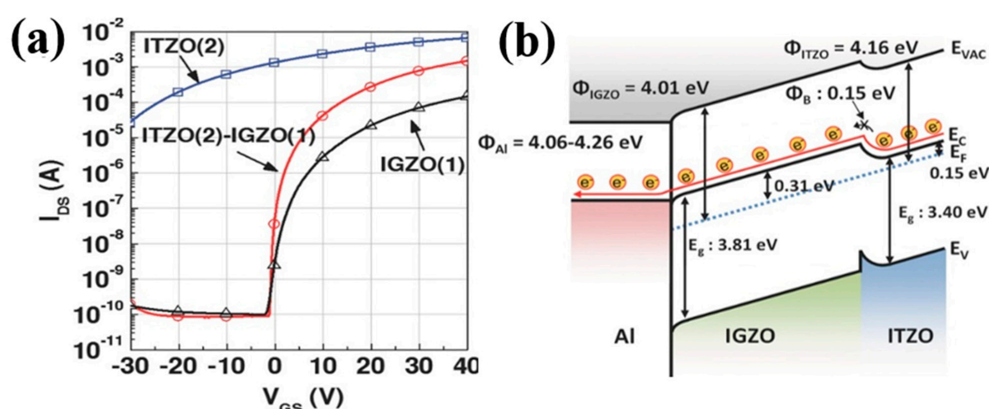

Figure 3. (**a**) Transfer characteristics of InGaZnO (IGZO), InSnZnO (ITZO), and ITZO/IGZO TFTs. (**b**) Energy band diagram of ITZO/IGZO. Reproduced with permission [51]. Copyright 2014, Wiley-VCH.

Nam et al. prepared high-performance solution-processed indium-free ZnO/SnO_2 TFTs at 300 °C by UV annealing [53]. The ZnO/SnO_2 TFTs exhibited a mobility of 15.4 cm^2/Vs, an outstanding on/off ratio of 10^8, and superior bias stability. As shown in Figure 4a, ZnO/SnO_2 bilayers are composed of a Zn-rich layer, a Zn-Sn mixed zone, and an Sn-rich layer. The Sn-rich channel has high conductivity and provides a path for rapid electronic transport. Meanwhile, Zn atoms can diffuse into the Zn-Sn mixing zone to reduce I_{off} by control carrier concentration. Furthermore, due to the suppression of oxygen vacancy (V_o) defects in the bilayer film, the ZnO/SnO_2 TFTs exhibited remarkable bias-stress stability (Figure 4b).

2.2.2. Mobility Enhancement by Forming 2D Electron Gas

In addition to electrical-performance modulation, some recent studies suggest that well-designed heterojunction oxides could greatly boost mobility by forming 2D electron gas at the interface [52]. Through careful interface engineering, electron transfer and confinement at the heterointerface can occur because of a large conduction band offset between the two layers, resulting in the formation of 2D

electron gas in the interface [55]. The formation of 2D electron gas enables the realization of TFTs with mobilities close to the theoretical limit set by phonon scattering in the absence of impurity scattering [30]. In this situation, the mobility of the heterojunction device is often several times or even ten times higher than that of the single-layer device. Additionally, the enhanced electron mobility is accompanied by a marked change in the charge transport mechanism. Through fitting the transfer curves and analyzing the temperature dependence of mobility, it was revealed that heterojunction TFTs exhibited band-like electron transport, while the single-layer device showed trap-limited conduction [55]. It should be mentioned that the transfer curve of the heterojunction TFTs shifted to the negative direction compared with the single-layer device, due to the formation of 2D electron gas.

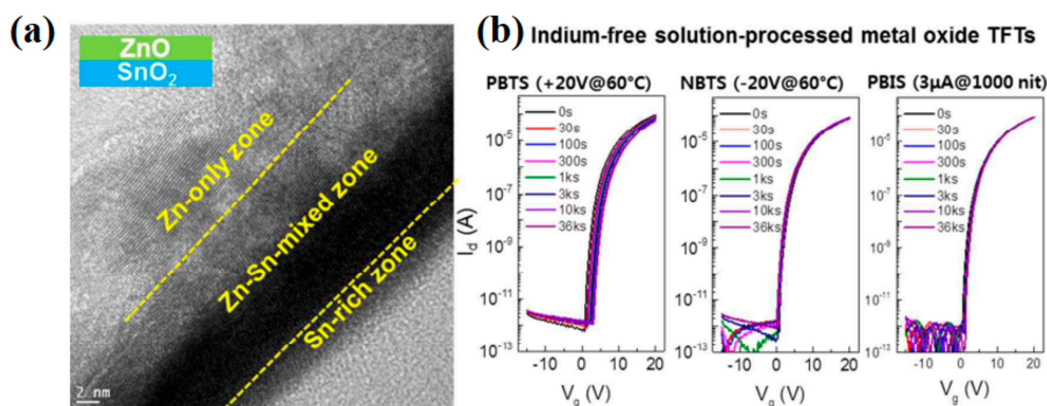

Figure 4. (**a**) Transmission electron microscope (TEM) of ZnO/SnO_2 heterojunction thin film. (**b**) Transfer curve evolutions for ZnO/SnO_2 heterojunction TFTs against a variety of bias stresses. Reproduced with permission [53]. Copyright 2016, Royal Society of Chemistry.

Faber et al. demonstrated In_2O_3/ZnO TFTs with unprecedented electron mobility grown from the solution [55]. The mobility of In_2O_3/ZnO TFTs (45 cm^2/Vs) was 2 to 100 times greater than that of single-layer In_2O_3 and ZnO devices. According to X-ray photoelectron spectroscopy, optical absorption, and Kelvin probe measurements, the In_2O_3/ZnO interface has a large conduction band offset (0.36 eV), which makes the electron transfer from the ZnO layer to In_2O_3 and forms 2D electron gas. 2D electron gas greatly increases the concentration of free electrons in the In_2O_3 layer of the crystal. The electron transport mechanism of In_2O_3/ZnO TFTs was changed from trap-limited conduction to percolation conduction. This marked improvement originated from the presence of 2D electron gas formed at the atomically sharp heterointerface induced by the large conduction band offset between In_2O_3 and ZnO. The In_2O_3/ZnO TFTs developed in this work not only surpassed the performance of single-layer In_2O_3 and ZnO TFTs but also compared favorably to state-of-the-art vacuum-processed devices. Lin et al. used solution-grown In_2O_3, Ga_2O_3, and ZnO to construct heterojunction and quasi-superlattice (QSL) TFTs (Figure 5a) [52]. By carefully optimizing the structure, QSLs with smooth interfaces and surfaces could be realized (Figure 5b). As shown in Figure 5c, it was proved that single-layer metal oxide TFTs were dominated by trap-limited conduction (TLC), while QSL-I/III were dominated by percolation conduction (PC). The change of electron transport mode led to a great increase in electron mobility (from 4 to 30 cm^2/Vs).

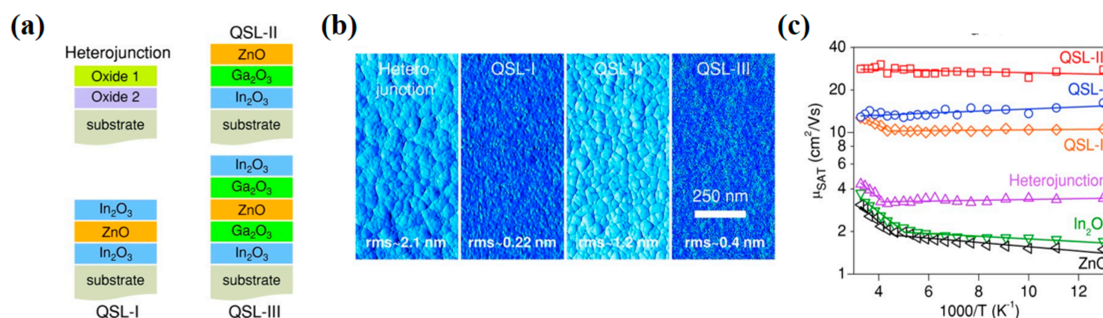

Figure 5. (**a**) Thin-film schematics of heterojunction quasi-superlattices (QSLs) consisting of $In_2O_3/ZnO/In_2O_3$ (QSL-I), $In_2O_3/Ga_2O_3/ZnO$ (QSL-II), and $In_2O_3/Ga_2O_3/ZnO/Ga_2O_3/In_2O_3$ (QSL-III). (**b**) Atomic force microscope (AFM) surface phase images of the different layered structures. (**c**) Arrhenius plots of the temperature dependence of the electron mobility for different layered structures. Reproduced with permission [52]. Copyright 2015, Wiley-VCH.

Later studies showed that layer configuration and annealing temperature greatly affect heterojunction device performance. Khim explored the effect of layer configuration on electron transport in heterojunction transistors composed of ZnO and In_2O_3 [57]. They found that depositing In_2O_3 first followed by ZnO resulted in a smooth interface, while reversing the layer order yielded poor interface roughness. Tetzner et al. studied the influence of annealing temperature on morphology, chemical state, and electrical performance of solution-based heterostructure In_2O_3/ZnO TFTs [54]. It was found that the annealing temperature changed surface roughness and atomic diffusion at the interface of In_2O_3/ZnO. At the annealing temperature of 400 °C, the In_2O_3/ZnO TFTs showed an optimized mobility of 48 cm^2/Vs and an on/off current ratio of ~10^4.

The large conduction band offset between the two layers is one of the key points to induce 2D electron gas for mobility improvement. A doping strategy has been adopted to enlarge the conduction band offset between the two layers. Khim and co-workers reported the controlled growth of In_2O_3/Li-ZnO TFTs by modulation doping [29]. It was revealed that Li addition in ZnO led to n-type doping and allowed for the accurate tuning of its Fermi energy. Therefore, doping of Li could precisely regulate ΔE_F between In_2O_3 and Li-ZnO and change the conduction band offset between the two layers (Figure 6). When the doping amount of Li was 20%, the mobility of In_2O_3/Li-ZnO heterojunction TFTs reached the maximum value of 11.4 cm^2/Vs and the on/off current ratio of ~10^5. Chen et al. demonstrated high performance In_2O_3/In_2O_3:polyethylenimine (PEI) heterostructure TFTs [56]. The 2D electron gas was achieved by creating a band offset between In_2O_3 and In_2O_3:PEI via work function tuning of the PEI-doping ratio. The resulting device exhibited a mobility of 10 cm^2/Vs on SiO_2 gate dielectric. Similarly, Liu et al. took In_2O_3 as the front channel and combined it with the back-channel AlInO to construct heterojunction transistors. By adjusting the thickness of AlInO and the doping amount of Al, AlInO (30%)/In_2O_3 heterostructure TFTs with a high mobility of 40 cm^2/Vs, a threshold slope of 0.7 V/dec, and an on/off ratio of 10^7 could be realized [58].

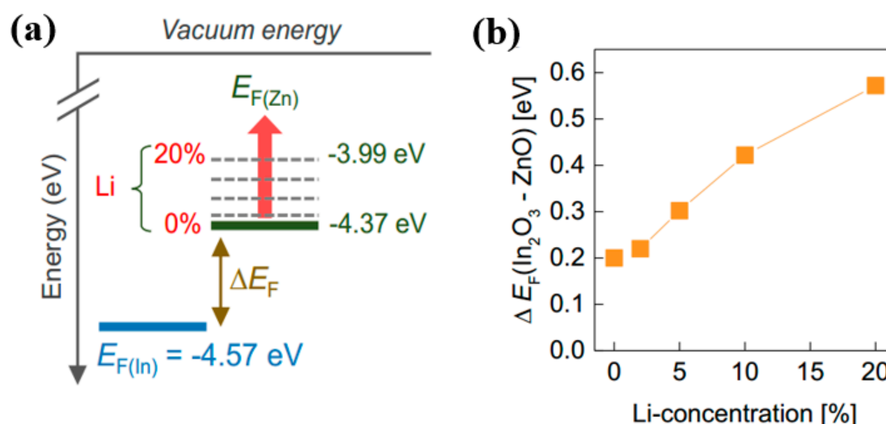

Figure 6. (**a**) Evolution of the Fermi energy level in In_2O_3 and ZnO layers as a function of Li concentration. (**b**) Schematic energy band diagram illustrating the shift of $E_{F(Zn)}$ to higher energies with increasing Li concentration in relation to $E_{F(In)}$. Reproduced with permission [29]. Copyright 2017, Wiley-VCH.

3. Conclusions and Outlooks

Great progress has been made in the past few years in solution-processed heterojunction oxide TFTs. A detailed review of this topic has been presented, with special attention on the latest developments over the past 5 years. It was revealed that heterojunction channels could overcome the disadvantages of single-layer structures. By using this novel strategy, solution-based oxide transistors with high mobility (~50 cm^2/Vs) and operational stability could be realized, competing with or even surpassing vacuum-grown counterparts.

In terms of future research directions, several key issues need to be addressed. First, the reported high mobility heterojunction oxide TFTs often suffered from negative threshold voltages, high off-state currents, or poor stability, which have a negative impact on commercial applications. The negative threshold voltage and high off-state current of heterojunction oxide TFTs are closely related to the formation of 2D electron gas. Lee et al. constructed corrugated structure ITZO/IGZO TFTs with both high mobility (51 cm^2/Vs) and low off-state current [30]. The thin ITZO/IGZO portion increased the overall resistivity of the current path, effectively reducing the off-state current. The thick ITZO/IGZO could provide free electrons to form a high-speed electronic channel, highly improving the electron mobility. By using this new corrugated heterojunction, solution-based oxide TFTs with high mobility and low off current could be realized. Unfortunately, this could increase the complexity of the process. Lin et al. reported solution-processed ZnO/ZnO-NPs/PS/In_2O_3 multilayer TFTs with high electron mobility (50 cm^2/Vs) and prolonged operational stability [31]. Insertion of the ozone-treated polystyrene interlayer could passivate electron traps in the channel, leading to high mobility and excellent operational stability. However, continued work should be carried out. It should be mentioned that well-optimized single-layer vacuum-based metal oxide TFTs show high performance and stability. Secondly, previous studies argued that the mobility enhancement is attributed to the 2D electron gas that formed at the heterogeneous interface. However, the traditional 2D electron gas usually exists in high-quality epitaxial heterojunction systems (such as AlGaAs/GaAs heterojunctions). The oxide thin films prepared by the solution method are usually polycrystalline or amorphous, and the 2D electron gas formation mechanism is still unclear. Thirdly, the carrier transport properties in heterojunction oxide need further investigation. A deep understanding of the heterojunction electron transport can promote better design of high-performance heterojunction oxide devices. Fourthly, the previous research mainly focused on the In_2O_3/ZnO system; it is necessary to extend this to other multicomponent oxide semiconductor heterostructures (such as the IGZO system) for further device performance improvement. We believe that by addressing the issues presented above, solution-processed heterojunction oxide TFTs will show great promise in future large-area and high-performance electronics.

Author Contributions: W.X. conceived and supervised the project. Y.L. (Yanwei Li) and W.X. wrote the manuscript. Y.L. (Yanwei Li), C.Z., D.Z., P.C., S.H., Y.L. (Youming Lu), M.F., W.L. and W.X. revised and commented on the manuscript. All authors have read and agreed to the published version of the manuscript.

Funding: This research was funded by National Natural Science Foundation of China (61704111, 51872187, 51371120 and 11774241), Natural Science Foundation of Guangdong Province (2017A030310524) and Science and Technology Foundation of Shenzhen (JCYJ20170817100611468 and JCYJ20170818143417082).

Conflicts of Interest: There are no conflicts to declare.

References

1. Yu, X.; Marks, T.J.; Facchetti, A. Metal oxides for optoelectronic applications. *Nat. Mater.* **2016**, *15*, 383. [CrossRef]
2. Fortunato, E.; Barquinha, P.; Martins, R. Oxide semiconductor thin-film transistors: A review of recent advances. *Adv. Mater.* **2012**, *24*, 2945–2986. [CrossRef] [PubMed]
3. Park, J.C.; Kim, S.; Kim, S.; Kim, C.; Song, I.; Park, Y.; Jung, U.I.; Kim, D.H.; Lee, J.S. Highly stable transparent amorphous oxide semiconductor thin-film transistors having double-stacked active layers. *Adv. Mater.* **2010**, *22*, 5512–5516. [CrossRef] [PubMed]
4. Pasquarelli, R.M.; Ginley, D.S.; Ryan, O.H. Solution processing of transparent conductors: From flask to film. *Chem. Soc. Rev.* **2015**, *43*, 5406–5441. [CrossRef] [PubMed]
5. Xu, W.; Li, H.; Xu, J.-B.; Wang, L. Recent Advances of Solution-Processed Metal Oxide Thin-Film Transistors. *ACS Appl. Mater. Interfaces* **2018**, *10*, 25878–25901. [CrossRef]
6. Chong, E.; Jeon, Y.W.; Chun, Y.S.; Kim, D.H.; Lee, S.Y. Localization effect of a current-path in amorphous In–Ga–Zn–O thin film transistors with a highly doped buried-layer. *Thin Solid Film.* **2011**, *519*, 4347–4350. [CrossRef]
7. Wakana, H.; Kawamura, T.; Fujii, K.; Uchiyama, H.; Hatano, M. P-17: Amorphous ZTO/ITO Stacked-Channel TFTs with Field Effect Mobility over 50 cm^2/Vs and Resistant to Channel Thickness Dispersion. *Sid Symp. Dig. Tech. Pap.* **2010**, *41*, 1287–1290. [CrossRef]
8. Liu, G.; Ao, L.; Zhu, H.; Shin, B.; Shan, F. Low-Temperature, Nontoxic Water-Induced Metal-Oxide Thin Films and Their Application in Thin-Film Transistors. *Adv. Funct. Mater.* **2015**, *25*, 2564–2572. [CrossRef]
9. Han, S.Y.; Herman, G.S.; Chang, C.H. Low-Temperature, High-Performance, Solution-Processed Indium Oxide Thin-Film Transistors. *J. Am. Chem. Soc.* **2011**, *133*, 5166. [CrossRef]
10. Marrs, M.A.; Moyer, C.D.; Bawolek, E.J.; Cordova, R.J.; Trujillo, J.; Raupp, G.B.; Vogt, B.D. Control of Threshold Voltage and Saturation Mobility Using Dual-Active-Layer Device Based on Amorphous Mixed Metal–Oxide–Semiconductor on Flexible Plastic Substrates. *IEEE Trans. Electron Devices* **2011**, *58*, 3428–3434. [CrossRef]
11. Jeon, S.; Sun, I.K.; Park, S.; Song, I.; Kim, C. Low-Frequency Noise Performance of a Bilayer InZnO–InGaZnO Thin-Film Transistor for Analog Device Applications. *IEEE Electron Device Lett.* **2010**, *31*, 1128–1130. [CrossRef]
12. Yang, J.H.; Choi, J.H.; Pi, J.E.; Kim, H.O.; Park, E.S.; Kwon, O.S.; Nam, S.; Cho, S.H.; Yoo, S.; Hwang, C.S. High Performance Back Channel Etch Metal Oxide Thin-film Transistor with Double Active Layers. *Sid Int. Symp. Dig. Technol. Pap.* **2016**, *47*, 1151–1154. [CrossRef]
13. Kim, H.S.; Park, J.S.; Jeong, H.K.; Son, K.S.; Kim, T.S.; Seon, J.B.; Lee, E.; Chung, J.G.; Kim, D.H.; Ryu, M.; et al. Density of states-based design of metal oxide thin-film transistors for high mobility and superior photostability. *ACS Appl. Mater. Interfaces* **2012**, *4*, 5416–5421. [CrossRef] [PubMed]
14. Kim, Y.H.; Heo, J.S.; Kim, T.H.; Park, S.; Yoon, M.H.; Kim, J.; Oh, M.S.; Yi, G.R.; Noh, Y.Y.; Park, S.K. Flexible metal-oxide devices made by room-temperature photochemical activation of sol-gel films. *Nature* **2012**, *489*, 128–132. [CrossRef] [PubMed]
15. Li, Y.; Zhu, D.; Xu, W.; Han, S.; Fang, M.; Liu, W.; Cao, P.; Lu, Y. High-mobility nanometer-thick crystalline In–Sm–O thin-film transistors via aqueous solution processing. *J. Mater. Chem. C* **2020**, *8*, 310–318. [CrossRef]
16. Jeong, S.; Ha, Y.G.; Moon, J.; Facchetti, A.; Marks, T.J. Role of gallium doping in dramatically lowering amorphous-oxide processing temperatures for solution-derived indium zinc oxide thin-film transistors. *Adv. Mater.* **2010**, *22*, 1346. [CrossRef] [PubMed]

17. Liang, K.; Wang, Y.; Shao, S.; Luo, M.; Pecunia, V.; Shao, L.; Zhao, J.; Chen, Z.; Mo, L.; Cui, Z. High-performance metal-oxide thin-film transistors based on inkjet-printed self-confined bilayer heterojunction channels. *J. Mater. Chem. C* **2019**, *7*, 6169–6177. [CrossRef]
18. Hennek, J.W.; Jeremy, S.; Aiming, Y.; Myung-Gil, K.; Wei, Z.; Dravid, V.P.; Antonio, F.; Marks, T.J. Oxygen "getter" effects on microstructure and carrier transport in low temperature combustion-processed a-InXZnO (X = Ga, Sc, Y, La) transistors. *J. Am. Chem. Soc.* **2013**, *135*, 10729–10741. [CrossRef]
19. Glynn, C.; O'Dwyer, C. Solution Processable Metal Oxide Thin Film Deposition and Material Growth for Electronic and Photonic Devices. *Adv. Mater. Interfaces* **2017**, *4*, 1600610. [CrossRef]
20. Garlapati, S.K.; Divya, M.; Breitung, B.; Kruk, R.; Dasgupta, S. Printed Electronics Based on Inorganic Semiconductors: From Processes and Materials to Devices. *Adv. Mater.* **2018**, *30*, 1707600. [CrossRef]
21. Seo, J.S.; Jeon, J.H.; Hwang, Y.H.; Park, H.; Ryu, M.; Park, S.H.; Bae, B.S. Solution-processed flexible fluorine-doped indium zinc oxide thin-film transistors fabricated on plastic film at low temperature. *Sci. Rep.* **2013**, *3*, 2085. [CrossRef] [PubMed]
22. Hsu, H.-H.; Chang, C.-Y.; Cheng, C.-H.; Chiou, S.-H.; Huang, C.-H. High Mobility Bilayer Metal–Oxide Thin Film Transistors Using Titanium-Doped InGaZnO. *IEEE Electron Device Lett.* **2014**, *35*, 87–89. [CrossRef]
23. Jung, H.Y.; Kang, Y.; Hwang, A.Y.; Lee, C.K.; Han, S.; Kim, D.H.; Bae, J.U.; Shin, W.S.; Jeong, J.K. Origin of the improved mobility and photo-bias stability in a double-channel metal oxide transistor. *Sci. Rep.* **2014**, *4*, 3765. [CrossRef] [PubMed]
24. Liu, G.X.; Liu, A.; Shan, F.K.; Meng, Y.; Shin, B.C.; Fortunato, E.; Martins, R. High-performance fully amorphous bilayer metal-oxide thin film transistors using ultra-thin solution-processed ZrOx dielectric. *Appl. Phys. Lett.* **2014**, *105*, 113509. [CrossRef]
25. Yang, C.P.; Chang, S.J.; Chang, T.H.; Wei, C.Y.; Juan, Y.M.; Chiu, C.J.; Weng, W.Y. Thin-Film Transistors With Amorphous Indium–Gallium-Oxide Bilayer Channel. *IEEE Electron Device Lett.* **2017**, *38*, 572–575. [CrossRef]
26. Kim, K.M.; Jeong, W.H.; Kim, D.L.; Rim, Y.S.; Choi, Y.; Ryu, M.-K.; Park, K.-B.; Kim, H.J. Low-Temperature Solution Processing of AlInZnO/InZnO Dual-Channel Thin-Film Transistors. *IEEE Electron Device Lett.* **2011**, *32*, 1242–1244. [CrossRef]
27. Park, J.C.; Lee, H.-N. Improvement of the Performance and Stability of Oxide Semiconductor Thin-Film Transistors Using Double-Stacked Active Layers. *IEEE Electron Device Lett.* **2012**, *33*, 818–820. [CrossRef]
28. Lee, J.; Lee, J.; Park, J.; Lee, S.E.; Lee, E.G.; Im, C.; Lim, K.H.; Kim, Y.S. Solution-Grown Homojunction Oxide Thin-Film Transistors. *ACS Appl. Mater. Interfaces* **2019**, *11*, 4103–4110. [CrossRef]
29. Khim, D.; Lin, Y.H.; Nam, S.; Faber, H.; Tetzner, K.; Li, R.; Zhang, Q.; Li, J.; Zhang, X.; Anthopoulos, T.D. Modulation-Doped In_2O_3/ZnO Heterojunction Transistors Processed from Solution. *Adv. Mater.* **2017**, 29. [CrossRef]
30. Lee, M.; Jo, J.W.; Kim, Y.J.; Choi, S.; Kwon, S.M.; Jeon, S.P.; Facchetti, A.; Kim, Y.H.; Park, S.K. Corrugated Heterojunction Metal-Oxide Thin-Film Transistors with High Electron Mobility via Vertical Interface Manipulation. *Adv. Mater.* **2018**, e1804120. [CrossRef]
31. Lin, Y.-H.; Li, W.; Faber, H.; Seitkhan, A.; Hastas, N.A.; Khim, D.; Zhang, Q.; Zhang, X.; Pliatsikas, N.; Tsetseris, L.; et al. Hybrid organic–metal oxide multilayer channel transistors with high operational stability. *Nat. Electron.* **2019**, *2*, 587–595. [CrossRef]
32. Yang, J.-H.; Choi, J.H.; Cho, S.H.; Pi, J.-E.; Kim, H.-O.; Hwang, C.-S.; Park, K.; Yoo, S. Highly Stable AlInZnSnO and InZnO Double-Layer Oxide Thin-Film Transistors With Mobility Over 50 cm/vs for High-Speed Operation. *IEEE Electron Device Lett.* **2018**, *39*, 508–511. [CrossRef]
33. Chen, X.; Wan, J.; Wu, H.; Liu, C. ZnO bilayer thin film transistors using H_2O and O_3 as oxidants by atomic layer deposition. *Acta Mater.* **2020**, *185*, 204–210. [CrossRef]
34. Tian, Y.; Han, D.; Zhang, S.; Huang, F.; Shan, D.; Cong, Y.; Cai, J.; Wang, L.; Zhang, S.; Zhang, X.; et al. High-performance dual-layer channel indium gallium zinc oxide thin-film transistors fabricated in different oxygen contents at low temperature. *Jpn. J. Appl. Phys.* **2014**, *53*, 04EF07. [CrossRef]
35. Abliz, A.; Huang, C.W.; Wang, J.; Xu, L.; Liao, L.; Xiao, X.; Wu, W.W.; Fan, Z.; Jiang, C.; Li, J.; et al. Rational Design of ZnO:H/ZnO Bilayer Structure for High-Performance Thin-Film Transistors. *ACS Appl. Mater. Interfaces* **2016**, *8*, 7862–7868. [CrossRef]
36. Cong, Y.; Han, D.; Zhou, X.; Huang, L.; Shi, P.; Yu, W.; Zhang, Y.; Zhang, S.; Zhang, X.; Wang, Y. High-Performance Al–Sn–Zn–O Thin-Film Transistor With a Quasi-Double-Channel Structure. *IEEE Electron Device Lett.* **2016**, *37*, 53–56. [CrossRef]

37. Sun Il, K.; Jung, K.C.; Chul, P.J.; Ihun, S.; Wook, K.S.; Huaxiang, Y.; Eunha, L.; Chul, L.J.; Youngsoo, P. High performance oxide thin film transistors with double active layers. In Proceedings of the 2008 IEEE International Electron Devices Meeting, San Francisco, CA, USA, 15–17 December 2008; pp. 1–4.
38. Chen, Z.; Han, D.; Zhao, N.; Cong, Y.; Jing, W.; Dong, J.; Zhao, F.; Liu, L.; Zhang, S.; Xing, Z. High-performance dual-layer channel ITO/TZO/TFTs fabricated on glass substrate. *Electron. Lett.* **2014**, *50*, 633–635. [CrossRef]
39. He, J.; Li, G.; Lv, Y.; Wang, C.; Liu, C.; Li, J.; Flandre, D.; Chen, H.; Guo, T.; Liao, L. Defect Self-Compensation for High-Mobility Bilayer InGaZnO/In_2O_3Thin-Film Transistor. *Adv. Electron. Mater.* **2019**, *5*, 1900125. [CrossRef]
40. Furuta, M.; Koretomo, D.; Magari, Y.; Aman, S.G.M.; Higashi, R.; Hamada, S. Heterojunction channel engineering to enhance performance and reliability of amorphous In–Ga–Zn–O thin-film transistors. *Jpn. J. Appl. Phys.* **2019**, *58*, 090604. [CrossRef]
41. Kim, J.-I.; Hwan Ji, K.; Yoon Jung, H.; Yeob Park, S.; Choi, R.; Jang, M.; Yang, H.; Kim, D.-H.; Bae, J.-U.; Dong Kim, C.; et al. Improvement in both mobility and bias stability of ZnSnO transistors by inserting ultra-thin InSnO layer at the gate insulator/channel interface. *Appl. Phys. Lett.* **2011**, *99*, 122102. [CrossRef]
42. Chong, E.; Lee, S.Y. Influence of a highly doped buried layer for HfInZnO thin-film transistors. *Semicond. Sci. Technol.* **2012**, *27*, 012001. [CrossRef]
43. Jo, K.-W.; Moon, S.-W.; Cho, W.-J. Fabrication of high-performance ultra-thin-body SnO_2 thin-film transistors using microwave-irradiation post-deposition annealing. *Appl. Phys. Lett.* **2015**, *106*, 043501. [CrossRef]
44. Lin, Y.Y.; Hsu, C.C.; Tseng, M.H.; Shyue, J.J.; Tsai, F.Y. Stable and High-Performance Flexible ZnO Thin-Film Transistors by Atomic Layer Deposition. *Acs Appl. Mater. Interfaces* **2015**, *7*, 22610–22617. [CrossRef] [PubMed]
45. Park, J.W.; Kang, B.H.; Kim, H.J. A Review of Low-Temperature Solution-Processed Metal Oxide Thin-Film Transistors for Flexible Electronics. *Adv. Funct. Mater.* **2019**, 1904632. [CrossRef]
46. Jeong, W.H.; Kim, K.M.; Kim, D.L.; Rim, Y.S.; Kim, H.J. The Effects of Dual-Active-Layer Modulation on a Low-Temperature Solution-Processed Oxide Thin-Film Transistor. *IEEE Trans. Electron Devices* **2012**, *59*, 2149–2152. [CrossRef]
47. Kim, D.J.; Rim, Y.S.; Kim, H.J. Enhanced electrical properties of thin-film transistor with self-passivated multistacked active layers. *ACS Appl. Mater. Interfaces* **2013**, *5*, 4190–4194. [CrossRef]
48. Kim, C.H.; Rim, Y.S.; Kim, H.J. Chemical stability and electrical performance of dual-active-layered zinc-tin-oxide/indium-gallium-zinc-oxide thin-film transistors using a solution process. *ACS Appl. Mater. Interfaces* **2013**, *5*, 6108–6112. [CrossRef]
49. Yu, X.; Zhou, N.; Smith, J.; Lin, H.; Stallings, K.; Yu, J.; Marks, T.J.; Facchetti, A. Synergistic approach to high-performance oxide thin film transistors using a bilayer channel architecture. *ACS Appl. Mater. Interfaces* **2013**, *5*, 7983–7988. [CrossRef]
50. Seo, J.S.; Bae, B.S. Improved electrical performance and bias stability of solution-processed active bilayer structure of indium zinc oxide based TFT. *ACS Appl. Mater. Interfaces* **2014**, *6*, 15335–15343. [CrossRef]
51. Rim, Y.S.; Chen, H.; Kou, X.; Duan, H.S.; Zhou, H.; Cai, M.; Kim, H.J.; Yang, Y. Boost up mobility of solution-processed metal oxide thin-film transistors via confining structure on electron pathways. *Adv. Mater.* **2014**, *26*, 4273–4278. [CrossRef]
52. Lin, Y.H.; Faber, H.; Labram, J.G.; Stratakis, E.; Sygellou, L.; Kymakis, E.; Hastas, N.A.; Li, R.; Zhao, K.; Amassian, A.; et al. High Electron Mobility Thin-Film Transistors Based on Solution-Processed Semiconducting Metal Oxide Heterojunctions and Quasi-Superlattices. *Adv. Sci.* **2015**, *2*, 1500058. [CrossRef] [PubMed]
53. Nam, S.; Yang, J.-H.; Cho, S.H.; Choi, J.H.; Kwon, O.-S.; Park, E.-S.; Lee, S.-J.; Cho, K.-I.; Jang, J.; Hwang, C.-S. Solution-processed indium-free ZnO/SnO_2 bilayer heterostructures as a low-temperature route to high-performance metal oxide thin-film transistors with excellent stabilities. *J. Mater. Chem. C* **2016**, *4*, 11298–11304. [CrossRef]
54. Tetzner, K.; Isakov, I.; Regoutz, A.; Payne, D.J.; Anthopoulos, T.D. The impact of post-deposition annealing on the performance of solution-processed single layer In_2O_3 and isotype In_2O_3/ZnO heterojunction transistors. *J. Mater. Chem. C* **2017**, *5*, 59–64. [CrossRef]
55. Faber, H.; Das, S.; Lin, Y.H.; Pliatsikas, N.; Zhao, K.; Kehagias, T.; Dimitrakopulos, G.; Amassian, A.; Patsalas, P.A.; Anthopoulos, T.D. Heterojunction oxide thin-film transistors with unprecedented electron mobility grown from solution. *Sci. Adv.* **2017**, *3*, e1602640. [CrossRef] [PubMed]

56. Chen, Y.; Huang, W.; Sangwan, V.K.; Wang, B.; Zeng, L.; Wang, G.; Huang, Y.; Lu, Z.; Bedzyk, M.J.; Hersam, M.C.; et al. Polymer Doping Enables a Two-Dimensional Electron Gas for High-Performance Homojunction Oxide Thin-Film Transistors. *Adv. Mater.* **2019**, *31*, e1805082. [CrossRef] [PubMed]
57. Khim, D.; Lin, Y.H.; Anthopoulos, T.D. Impact of Layer Configuration and Doping on Electron Transport and Bias Stability in Heterojunction and Superlattice Metal Oxide Transistors. *Adv. Funct. Mater.* **2019**, *29*, 1902591. [CrossRef]
58. Liu, L.; Chen, S.; Liang, X.; Pei, Y. Solution Processed AlInO/In_2O_3 Heterostructure Channel Thin Film Transistor with Enhanced Performance. *Adv. Electron. Mater.* **2019**, *5*, 1900550. [CrossRef]
59. Nadarajah, A.; Wu, M.Z.B.; Archila, K.; Kast, M.G.; Smith, A.M.; Chiang, T.H.; Keszler, D.A.; Wager, J.F.; Boettcher, S.W. Amorphous In–Ga–Zn Oxide Semiconducting Thin Films with High Mobility from Electrochemically Generated Aqueous Nanocluster Inks. *Chem. Mater.* **2015**, *27*, 5587–5596. [CrossRef]

© 2020 by the authors. Licensee MDPI, Basel, Switzerland. This article is an open access article distributed under the terms and conditions of the Creative Commons Attribution (CC BY) license (http://creativecommons.org/licenses/by/4.0/).